This is a preprint, the final version is subject to change, of the American Mineralogist (MSA)
Cite as Authors (Year) Title. American Mineralogist, in press.
DOI: https://doi.org/10.2138/am-2019-6842

REVISION 1

A Low-Aluminum Clinopyroxene-Liquid Geothermometer for High-Silica Magmatic Systems

Karalee K. Brugman
School of Earth and Space Exploration, Arizona State University
781 Terrace Mall, ISTB4, Room 795
Tempe, AZ 85287-6004, USA
(480) 727-2559
kara.brugman@asu.edu

Christy B. Till
School of Earth and Space Exploration, Arizona State University
781 Terrace Mall, ISTB4, Room 795
Tempe, AZ 85287-6004, USA
(480) 727-2828
christy.till@asu.edu

This is a preprint, the final version is subject to change, of the American Mineralogist (MSA)
Cite as Authors (Year) Title. American Mineralogist, in press.
DOI: https://doi.org/10.2138/am-2019-6842

Abstract

A number of geothermobarometric tools have focused on clinopyroxene due to its prevalence in igneous rocks, however clinopyroxene produced in high-silica igneous systems is high in iron and low in aluminum, causing existing geothermometers that depend on aluminum exchange to fail or yield overestimated temperatures. Here we present a new clinopyroxene-liquid geothermometer recommended for use in natural igneous systems with bulk $SiO_2 \geq 70$ wt%, which contain clinopyroxene with Mg# ≤ 65 and $Al_2O_3 \leq 7$ wt%

$$T[°C] = 300[-1.89 - 0.601\left(X_{CaTs}^{cpx}\right) - 0.186\left(X_{DiHd_{2003}}^{cpx}\right) + 4.71\left(X_{SiO_2}^{liq}\right) + 77.6\left(X_{TiO_2}^{liq}\right) + 10.9\left(X_{FeO}^{liq}\right) + 33.6\left(X_{MgO}^{liq}\right) + 15.5\left(X_{CaO}^{liq}\right) + 15.6\left(X_{KO_{0.5}}^{liq}\right)] \quad (1)$$

The new geothermometer lowers calculated temperatures by 85°C on average relative to Putirka (2008, Eq. 33) and reduces the uncertainty by a factor of two (standard error of estimate ± 20°C). When applied to natural systems, we find this new clinopyroxene-liquid geothermometer reconciles many inconsistencies between experimental phase equilibria and preexisting geothermometry results for silicic volcanism, including those from the Bishop Tuff and Yellowstone caldera-forming and post-caldera rhyolites. We also demonstrate that clinopyroxene is not restricted to near-liquidus temperatures in rhyolitic systems; clinopyroxene can be stable over a broad temperature range, often down to the solidus. An Excel spreadsheet and Python notebook for calculating temperature with this new geothermometer may be downloaded from GitHub at http://bit.ly/cpxrhyotherm.

Keywords: geothermometer, clinopyroxene, high-silica

Introduction

Investigations of igneous systems often begin with an assessment of the temperature during eruption, crystallization, and/or magma storage, and geothermometers are generally calibrated to work with a broad range of rock types and mineral compositions. At least 40 clinopyroxene geothermometers have been developed, and many improve on past geothermometers or build on a previously published activity model. Two-pyroxene geothermometers are the most common type (e.g., Lindsley and Andersen 1983; Anderson et al. 1993; Sack and Ghiorso 1994; Putirka 2008; Liang et al. 2013) and take advantage of the temperature-dependent solvus of the pyroxene system. But, these geothermometers necessitate the presence of equilibrium pairs of clinopyroxene and orthopyroxene in the host rock and are almost exclusively calibrated for diopside (Di; $CaMgSi_2O_6$), the low-Fe endmember of calcic clinopyroxene. Another type of geothermometer, clinopyroxene-liquid (e.g., Putirka 2008; Masotta et al. 2013), does not require co-crystallizing orthopyroxene and relies on the equilibria of Di, hedenbergite (Hd; $CaFeSi_2O_6$), and jadeite (Jd; $NaAlSi_2O_6$), the high-Al endmember of sodic clinopyroxene. However, geothermometers dependent on this equilibria are likely to be inaccurate if there is very little Al in the clinopyroxene and thus very little to no Jd component (which is calculated based on the estimated Al^{IV} rather than Na when Al^{IV} is low—see Supplementary Table 1). This caveat becomes significant when studying high-silica systems, in which clinopyroxene is typically high in Fe (up to 30 wt% oxide) and low in Al (< 2 wt% oxide; Figure 1).

Unfortunately, the high-Fe, low-Al clinopyroxene from high-silica systems are not well represented in experimental data used to calibrate existing geothermometers, as the majority of

experimental studies tend to explore Mg-rich augite to diopside, and in mafic rather than silicic systems. In silica-saturated systems, the major phases are Al-bearing plagioclase and alkali feldspar, and clinopyroxene have relatively low CaO; consequently, these clinopyroxene crystallize with almost all tetrahedral sites filled with Si rather than Al (Salviulo et al. 2000). A result of the historical sampling bias is that in Al_2O_3-Mg# space, there is no overlap between the clinopyroxene found in many natural high-silica magmatic systems and the clinopyroxene used to calibrate two of the most commonly used clinopyroxene geothermometers, the Putirka (2008) clinopyroxene-liquid geothermometer and the MELTS two-pyroxene geothermometer (Sack and Ghiorso 1994) (Figure 1). For many high-Fe, low-Al clinopyroxene, the most popular clinopyroxene-liquid geothermometer (Putirka 2008, Eq. 33) does not successfully calculate a temperature. When it does, it returns systematically high temperatures, up to 170°C greater than the conditions of high-Fe, low-Al clinopyroxene-saturated experiments, indicating that this geothermometer is not well suited for this restricted mineral composition. Thus, if we wish to utilize clinopyroxene in our thermal investigations of high-silica systems such as Long Valley, Yellowstone, and Valles Calderas, it is prudent to develop a new geothermometer that is calibrated for the clinopyroxene found in these eruptive products.

Here we present a new clinopyroxene-liquid geothermometer, calibrated using data from experiments on high-silica systems that crystallized high-Fe, low-Al clinopyroxene, that is able to consistently calculate temperatures where other geothermometers fail and reproduces experimental temperatures to within 17°C. Also, for high-silica system experiments below 850°C—the temperature range of most interest for these systems—the new clinopyroxene-liquid geothermometer offers a five-fold decrease in the deviation between calculated and actual experimental temperatures as compared to the Putirka (2008, Eq. 33) geothermometer (± 20°C

89 versus ± 110°C). We apply the geothermometer to a series of silicic igneous systems to examine
90 the effect of these adjusted temperatures on our petrologic understanding of phase relations and
91 magma storage conditions.
92
93 **Methods**
94 In order to calibrate a new geothermometer, a dataset of clinopyroxene and glass
95 compositions was compiled from recent experimental studies on high-silica magmatic systems
96 (Supplementary Table 2). The selected studies were conducted at 675–1025°C and 75–503 MPa
97 and yielded experimental run products with a bulk silica content of > 70 wt% and clinopyroxene
98 with ≤ 7 wt% Al_2O_3 and Mg# from 2.5–77 (Figure 1, Supplementary Table 2). These data
99 included relatively few experiments performed between 750–875°C, therefore new hydrothermal
100 cold-seal pressure vessel (CSPV) experiments (4) were conducted in this temperature range to
101 supplement the experiments from the literature.
102 For the new experiments, the starting material, the Scaup Lake rhyolite from
103 Yellowstone Caldera (sample 12CTYC-01), was twice powdered, homogenized, and glassed at
104 1400°C for 30 minutes in a 1 atm vertical furnace at the Experimental Petrology and Igneous
105 processes Center (EPIC) at Arizona State University (ASU) (Table 1). Single Scaup Lake
106 clinopyroxene crystals with intact, euhedral faces were hand-picked under stereo microscope
107 from a ≤ 1 mm size fraction of mineral separates in order to mitigate compositional
108 heterogeneity due to subtle intracrystalline zoning. These clinopyroxene were used as seed
109 crystals in the whole rock powder. The CSPV experiments were conducted at the Massachusetts
110 Institute of Technology experimental petrology lab in Stellite No. 25 cold-seal hydrothermal
111 pressure vessels with filler rods, and were heated in horizontal, split-tube furnaces. Temperatures

were monitored using chromel-alumel thermocouples. Experiments were H_2O-saturated and buffered at NNO using double Au capsules with powdered Ni-NiO buffer in the outer capsule. The pressure for all experiments was 1 kbar, run durations were ~16–24 days (Table 2), and experiments were quenched by blowing compressed air over the vessels while at pressure. After quenching, inner and outer capsules were weighed before and after they were pierced and dried in a warming oven for 10 minutes. If mass was lost after piercing and drying, often in conjunction with water visible upon piercing, the capsule was presumed to be H_2O-saturated.

The CSPV experimental products (Supplementary Table 2) were mounted in epoxy in wells drilled into 1" aluminum rounds and then measured on the JXA-8530F EPMA at ASU's Eyring Materials Center using an accelerating voltage of 15 kV and beam current of 15 nA. Beam sizes were 1 μm for clinopyroxene and 10 μm for glass. Time-dependent intensity (TDI) correction was applied to glass measurements of Na, K, and Si to mitigate migration of light elements away from the electron beam.

Results and Discussion

CSPV calibration experiments

Four successful experiments (750–825°C, 1 kbar) were glassy with bubbles and included amphibole, indicating the charges remained H_2O-saturated for the run duration. All experiments crystallized clinopyroxene (Figure 2, Supplementary Table 2) and contained equilibrated, unzoned seed crystals, with variable minor amounts of alkali feldspar, plagioclase, Fe-Ti oxides, and quartz.

Accepted clinopyroxene data were sourced from crystals that showed no zoning in backscattered electron (BSE) images. These data were from either newly grown crystals or rims

of equilibrated seed crystals (easily distinguished by size: <0.5 μm vs ≥100 μm) that differed from their starting composition (Supplementary Table 3).

Geothermometer calibration and performance

The CSPV experiment data were combined with the previously published experiment data (see Methods). 64 of these data points constitute the geothermometer calibration dataset of high-Fe, low-Al clinopyroxene and glass pairs (Table 3, Supplementary Table 2). 13 data points were not included in the calibration dataset and instead were set aside as a test dataset to check the efficacy of the geothermometer. To preserve temperature variation in the calibration data, a data point was excluded from the calibration dataset and reserved for the test dataset only if the experiment was conducted at the same temperature as other experiments in that particular study.

The calibration dataset clinopyroxene and glass compositions (60 previously published and 4 from this work) were converted to clinopyroxene components and liquid cation fractions following the procedure used in previous clinopyroxene-liquid geothermometers (Putirka et al. 2003 and references therein) (see Supplementary Table 1 for full procedure). Backwards step-wise regression was used to determine which parameters best explained the variation in experimental temperatures. Significant parameters were selected based on statistics of significance from preliminary linear regressions on the calibration dataset. These initial linear regressions were performed with T as the dependent variable, and one of two groups of parameters as independent variables. Parameter Group A was comprised of those calculated for use in the Putirka (2008, Eq. 33) geothermometer and Group B encompassed Group A as well as calculations of cations based on 6 oxygens for clinopyroxene (Supplementary Table 1). A

This is a preprint, the final version is subject to change, of the American Mineralogist (MSA)
Cite as Authors (Year) Title. American Mineralogist, in press.
DOI: https://doi.org/10.2138/am-2019-6842

parameter progressed to the next stage of the process if the 95% confidence interval for its coefficient did not include 0.

These limited sets of parameters were used in new linear regression trials to create new candidate geothermometer equations. These equations were evaluated for efficacy by their ability to return accurate temperatures from the test dataset (e.g., R^2 and standard error of estimate (SEE)). Ultimately, the parameters from both clinopyroxene and liquid that most improved regression statistics were sourced from Group A, resulting in the geothermometer equation:

$$T[°C] = 300[-1.89 - 0.601\left(X_{CaTs}^{cpx}\right) - 0.186\left(X_{DiHd_{2003}}^{cpx}\right) + 4.71\left(X_{SiO_2}^{liq}\right) + 77.6\left(X_{TiO_2}^{liq}\right) + 10.9\left(X_{FeO}^{liq}\right) + 33.6\left(X_{MgO}^{liq}\right) + 15.5\left(X_{CaO}^{liq}\right) + 15.6\left(X_{KO_{0.5}}^{liq}\right)] \quad (1)$$

$X_{DiHd_{2003}}^{cpx}$ represents the Di plus Hd components of clinopyroxene as described in Putirka et al. (2003), and $X_{SiO_2}^{liq}$ represents the cation fraction of SiO_2 in the liquid.

The new geothermometer reproduced the temperatures of the test dataset well, with an R^2 value of 0.95 as compared to $R^2 = 0.72$ for temperatures calculated using the Putirka (2008) clinopyroxene-liquid geothermometer (using Putirka 2008 Eq. 33 in concert with the reported experimental *P*) (Figure 3b). Based on results from the test dataset, the new geothermometer has an SEE of ± 20°C, and when applied to both the calibration and test dataset of high-Fe, low-Al experimental clinopyroxene, recovers these temperatures to within an average of 17°C. In comparison, the Putirka (2008, Eq. 33) geothermometer, which is calibrated for a broad range of systems, has a reported SEE of ± 45°C, and can overestimate the same experiments' temperatures by > 170°C. For experiments performed ≤ 850°C, the new geothermometer

This is a preprint, the final version is subject to change, of the American Mineralogist (MSA)
Cite as Authors (Year) Title. American Mineralogist, in press.
DOI: https://doi.org/10.2138/am-2019-6842

returned temperatures within an average of 20°C, a five-fold improvement over the Putirka (2008, Eq. 33) clinopyroxene-liquid geothermometer (Figure 3).

The new geothermometer eliminates any dependence on Jd, and the H_2O and pressure terms in the Putirka (2008, Eq. 33) geothermometer were found to have no significant effect on this empirical calibration. The only clinopyroxene parameters on which the geothermometer relies are the Ca-Tschermak's (CaTs) and $DiHd_{2003}$ components. The new geothermometer has a strong dependence on the TiO_2 and MgO content of the liquid, and greatly increases the dependence on SiO_2 and CaO in the liquid over that of the Putirka (2008, Eq. 33) geothermometer. Because of the new geothermometer's strong dependence on the liquid composition, for input conditions we recommend only using actual glass compositions measured as close as is prudent to the clinopyroxene of interest. This is in part because the rhyolitic whole rock oxide composition can deviate from that of the glass, particularly in those oxides used in the geothermometer e.g., MgO which tends to be higher in crystal cores. Using whole rock instead of glass compositions with the geothermometer increases the SEE of the calculated temperature. For example, a temperature calculated for Bishop Tuff samples using whole rock is > 60°C higher (> 3x the SEE) than a temperature calculated correctly with glass.

Calibration trials were also conducted using the same parameters as the Putirka (2008, Eq. 33) clinopyroxene-liquid geothermometer, including Jd and *P*. Although temperature estimates using these parameters were somewhat improved over the original Putirka (2008, Eq. 33) geothermometer (SEE ± 30°C vs. ± 60°C for our test dataset), this parameterization produced a lower R^2 than our new empirically-based regression equation (0.81 vs. 0.95) and the SEE was ~10°C greater (SEE ± 30°C vs. ± 20°C) for both the entire test dataset and the experiments performed ≤ 850°C. This result is not surprising, because although the Putirka (2008)

This is a preprint, the final version is subject to change, of the American Mineralogist (MSA)
Cite as Authors (Year) Title. American Mineralogist, in press.
DOI: https://doi.org/10.2138/am-2019-6842

202 geothermometer is thermodynamically motivated, it relies on Di, Hd, and Jd equilibria—the Jd
203 content of natural high-silica system clinopyroxene can be zero and the estimated Jd content of
204 the new geothermometer's calibration dataset is as low as 0.002.

205 Additionally, we explored a universal clinopyroxene-liquid geothermometer calibrated
206 with a dataset comprised of both our calibration dataset and that used to calibrate Putirka (2008,
207 Eq. 33). Although this geothermometer was able to return a temperature for all test data and
208 improved the SEE of experiments conducted ≤ 850 °C versus the original Putirka (2008, Eq. 33)
209 geothermometer, it was not pursued as it did not improve the SEE for the high-Fe, low-Al test or
210 calibration datasets. And, with $R^2 = 0.80$, the universal geothermometer had the poorest R^2 value
211 of any of the candidate geothermometer equations. This is also not surprising, as the two
212 calibration datasets—our high-Fe, low-Al clinopyroxene and Putirka (2008)'s generally more
213 mafic clinopyroxene—have little overlap in Al_2O_3 vs. Mg# space or on the pyroxene
214 quadrilateral (Figure 1).

215 Although the Putirka (2008, Eq. 33) clinopyroxene-liquid geothermometer was calibrated
216 to be broadly applied and is an excellent tool for use with the majority of igneous rock
217 compositions, including more augitic or high-Al clinopyroxene from high-silica systems, high-
218 Fe, low-Al clinopyroxene appear to be an end member case that requires special handling. For
219 high-Fe, low-Al clinopyroxene, a universal geothermometer is unable to match the accuracy of a
220 specialized tool.

221 In some cases, the temperatures calculated with the new geothermometer are within
222 uncertainty of the Putirka (2008, Eq. 33) geothermometer. However, the Putirka (2008)
223 geothermometer will sometimes fail to return a temperature for high-Fe, low-Al clinopyroxene,
224 particularly if Jd = 0 (i.e., when $Al^{IV} = 0$), and the new geothermometer eliminates this issue in

This is a preprint, the final version is subject to change, of the American Mineralogist (MSA)
Cite as Authors (Year) Title. American Mineralogist, in press.
DOI: https://doi.org/10.2138/am-2019-6842

addition to decreasing uncertainty. Although the new geothermometer calibration dataset clinopyroxene has median 2.25 wt% Al_2O_3 (23% of the dataset has < 1 wt%) it includes clinopyroxene with up to 7.08 wt% Al_2O_3 (Fig. 1). Thus, our new clinopyroxene-liquid geothermometer is recommended for use with natural systems that have bulk $SiO_2 \geq 70$ wt% and bear clinopyroxene with Mg# ≤ 65 and $Al_2O_3 \leq 7$ wt%. An Excel spreadsheet and Python notebook for calculating temperature with this new geothermometer are included in the Supplementary Materials. The most up to date version may be downloaded from GitHub at http://bit.ly/cpxrhyotherm.

Equilibrium of natural samples

An important question when considering using a clinopyroxene-liquid geothermometer is whether natural clinopyroxene are in equilibrium with coexisting liquid in natural samples. If the mineral did not crystallize in equilibrium with the liquid, results returned by a geothermometer that is based on these two compositions—such as ours—will be suspect. To investigate clinopyroxene-liquid equilibrium and provide a tool for assessing equilibrium in conjunction with our geothermometer, major element partition coefficients were calculated for all experimental compositions in the calibration dataset (n = 64), as well as for the larger dataset (n = 1290) used to calibrate the Putirka (2008) geothermometer. Using this combined experimental dataset, we find SiO_2 clinopyroxene-liquid partition coefficients to be a reliable indicator of equilibrium, with mafic samples having $Kd_{SiO_2}^{cpx-liquid} > 1.0$ (average = 1.03), rhyolitic samples having $Kd_{SiO_2}^{cpx-liquid} < 0.75$ (average = 0.68), and intermediate silica samples having intermediate $Kd_{SiO_2}^{cpx-liquid}$ values (average = 0.81). Thus, we advise using clinopyroxene-liquid pairs with our geothermometer only when the $Kd_{SiO_2}^{cpx-liquid}$ is < 0.75. The natural samples explored in the

discussion section have average $Kd_{SiO_2}^{cpx-liquid}$ = 0.66, indicating clinopyroxene is in equilibrium with rhyolitic liquids in these systems.

Application to Natural Systems

Here we use the new geothermometer to calculate temperatures for several natural high-silica systems (Table 4, Supplementary Table 3). In all cases the new geothermometer yields temperatures that are lower than those calculated with the Putirka (2008, Eq. 33) geothermometer; for the Bishop Tuff, Bandelier Tuff, and Paektu comendite, this difference is 130°C on average (Figure 4). For all high-silica systems considered, the new geothermometer calculates temperatures that are more consistent with our understanding of those systems, as well as with experimental phase equilibria and other mineral-derived temperatures.

Late-erupted Bishop Tuff, Long Valley

The 0.76 Ma Late-erupted Bishop Tuff (Ig2) was emplaced at Long Valley Caldera in eastern California near the end of an eruption whose eruptive products covered as much as $2.5x10^6$ km^2 of North America (Hildreth and Wilson 2007). The Bishop Tuff has been intensely studied (e.g., Hildreth 1977, 1981; Hervig and Dunbar 1992; Wilson and Hildreth 1997; Anderson et al. 2000; Bindeman and Valley 2002; Reid et al. 2011; Gualda and Ghiorso 2013; Chamberlain et al. 2014; Gualda and Sutton 2016) with particular interest in the possible stratification of the magma body before eruption, based on Fe-Ti oxide geothermometry. Fe-Ti oxide QUILF geothermometry (Anderson et al. 1993) of the later ignimbrite returns temperatures over 800°C and a temperature of ~720°C for the earlier units (Hildreth and Wilson 2007; Ghiorso and Evans 2008). Similarly, quartz-magnetite oxygen isotope geothermometry returns

815°C for the Late-erupted units and 715°C for the Early-erupted units (Bindeman and Valley 2002). However, Gardner et al. (2014) and Ghiorso and Gualda (2013) suggest that the Fe-Ti oxides did not crystallize in equilibrium with the rest of the Bishop Tuff phase assemblage, and that the oxygen isotope geothermometry may not reflect magmatic storage temperatures. Instead, Gardner et al. (2014) suggest a pre-eruptive storage temperature of < 740°C based on phase equilibria experiments on the Late-erupted Bishop Tuff composition.

Pyroxene phenocrysts are not present in the Early-erupted Bishop Tuff, but clinopyroxene is present in the Late-erupted Bishop Tuff (Table 4, Supplementary Table 3). Experimental studies of Late-erupted Bishop Tuff pumice containing 20% phenocrysts of quartz, sanidine, plagioclase, clinopyroxene, orthopyroxene, biotite, magnetite, and ilmenite indicate that clinopyroxene does not crystallize at temperatures above 800°C at pressures > 1.4 kbar and is unlikely to crystallize above 820°C at pressures ≤ 1.2 kbar (Adamukcu et al. 2012; Gardner et al. 2014). The Putirka (2008, Eq. 33) clinopyroxene-liquid geothermometer calculates 870°C for the Late-erupted Bishop Tuff natural clinopyroxene rims, which places the clinopyroxene crystallization interval far above the experimental liquidus of Gardner et al. (2014) (Figure 5). The new geothermometer calculates a Late-erupted clinopyroxene temperature of 759°C which is well within the clinopyroxene stability field in experimental studies and is also consistent with the Gardner et al. (2014) storage temperature and Ti-in-zircon geothermometry (Gualda and Ghiorso 2013) (Figure 5). The lower clinopyroxene temperature of 759°C is also closer to the Fe-Ti oxide and oxygen isotope temperatures for the Early-erupted units, lending support to the argument that this material may not have been stored at much higher temperatures than the Early-erupted products, and thus does not support a vertical stratification model for the Bishop Tuff magma body. Workers have suggested the pyroxene-free Early-erupted material may have

This is a preprint, the final version is subject to change, of the American Mineralogist (MSA)
Cite as Authors (Year) Title. American Mineralogist, in press.
DOI: https://doi.org/10.2138/am-2019-6842

294 been stored laterally to the Late-erupted material (Wilson and Hildreth 1997; Cashman and
295 Giordano 2014), and the new geothermometer results for the Bishop Tuff could lend credence to
296 this hypothesis.
297
298 **Millennium Eruption comendite, Paektu**
299 Paektu (also known as Changbaishan) is a high-silica igneous system located on the
300 border of the Democratic People's Republic of Korea and China. Circa 946 AD, the Paektu
301 Millennium Eruption deposited 23±5 km^3 DRE of tephra, most of which is comendite pumice
302 containing alkali feldspar, clinopyroxene (Table 4, Supplementary Table 3), fayalite, Fe-Ti
303 oxides, and quartz (Horn and Schmincke 2000). Phase equilibria experiments for this system
304 indicate that clinopyroxene is the liquidus phase, with the liquidus at ~720°C at 1 kbar and
305 ~770°C at 500 bar (Iacovino et al. 2015, 2016). Similar to the above results for the Bishop Tuff,
306 the Putirka (2008, Eq. 33) clinopyroxene-liquid geothermometer returns a superliquidus
307 temperature of 889°C for the Millennium Eruption comendite pumice, whereas the new
308 geothermometer yields a temperature of 755°C, which approximates the temperature
309 experimentally determined to best reproduce the natural phase assemblage (725°C at 500 bar;
310 Iacovino et al. 2015, 2016). Paektu is yet to be studied in depth, and it remains unclear whether
311 the Millennium Eruption was the caldera-forming eruption. The new clinopyroxene-liquid
312 geothermometer could help elucidate Paektu's history in future investigations.
313
314 **Scaup Lake rhyolite, Yellowstone**
315 High-Fe, low-Al clinopyroxene is the most abundant mafic phase in the Scaup Lake
316 rhyolite, a lava emplaced effusively ca. 257 ka, after the last caldera-forming eruption at

This is a preprint, the final version is subject to change, of the American Mineralogist (MSA)
Cite as Authors (Year) Title. American Mineralogist, in press.
DOI: https://doi.org/10.2138/am-2019-6842

Yellowstone (Christiansen et al. 2007; Girard and Stix 2009). Scaup Lake clinopyroxene (Table 4, Supplementary Table 3) exhibit exsolution lamellae, are reverse zoned with higher-Fe cores, and have alternating higher- and lower-Fe fine rim zones, all indicators of a complex pre-eruptive history involving both thermal and chemical variation (Till et al. 2015). The Putirka (2008, Eq. 33) clinopyroxene-liquid geothermometer was unable to calculate temperatures for a number of Scaup Lake clinopyroxene-liquid pairs because the Scaup Lake clinopyroxene have, on average, Jd < 0.008. The new clinopyroxene-liquid geothermometer yields a temperature of 800°C for the outermost rim of these clinopyroxene, which is slightly lower than that of the Putirka (2008, Eq. 33) geothermometer (827°C when able to be calculated) and much lower than the two-pyroxene temperature of ~880°C obtained via PyMELTS (Sack and Ghiorso 1994) and QUILF. Other post-caldera lavas from Yellowstone, the South Biscuit Basin and Solfatara Plateau rhyolites emplaced ca. 255 and 103 ka, respectively (Christiansen 2001; Bindeman et al. 2008), yield new geothermometer temperatures ~80°C lower than the temperatures calculated by the Putirka (2008, Eq. 33) clinopyroxene-liquid geothermometer (Figure 4), underlining the importance of using the new geothermometer for the Yellowstone system.

We judge the new temperature to be the preferred temperature for Scaup Lake clinopyroxene rim growth because, unlike the Putirka (2008, Eq. 33) clinopyroxene-liquid geothermometer, the new geothermometer is able to calculate temperatures for all Scaup Lake clinopyroxene compositions and does not rely on the presence of co-crystallizing orthopyroxene, so it can be used if there is any uncertainty about phase equilibria. This temperature is slightly lower than that recorded by prior Fe-Ti oxide geothermometry (834–880°C: Hildreth et al. 1984; Vazquez et al. 2009) and two-feldspar geothermometry (819±20°C: Till et al. 2015), differences we do not interpret as an error in geothermometry, but rather as a reflection of the relative

location of phase boundaries and a particular mineral-element pair's ability to diffusively re-equilibrate.

For example, Scaup Lake quartz return temperatures of 849±13°C for cores and 862±10°C for rims (Vazquez et al. 2009) via TitaniQ (Wark and Watson 2006). The new geothermometer's clinopyroxene rim temperature of 800°C indicates that clinopyroxene continues to crystallize at or below the temperatures of the quartz-in phase boundary for the Scaup Lake rhyolite. Although there are questions as to the effect of growth rate and a_{TiO2} on TitaniQ (e.g., Huang and Audétat 2012; Ghiorso and Gualda 2013; Pamukcu et al. 2016), this is the same relative positioning of the quartz-in and clinopyroxene-in phase boundaries observed in experiments on other similar composition systems such as the Blacktail Creek Tuff (Bolte et al. 2015) and Solfatara Plateau rhyolite (Befus and Gardner 2016).

The 800°C rim crystallization temperature returned by the new geothermometer is also more consistent with our understanding of how exsolution lamellae form parallel to [100] in the cores of clinopyroxene, a feature that is observed in the Scaup Lake clinopyroxene. Experimental studies show that orthopyroxene-in-augite lamellae require temperatures below 825°C to form (Huebner 1980; Lindsley 1983). Temperatures calculated for Scaup Lake by other methods are too high to account for the formation of the lamellae, e.g., 862±36°C (Shaffer and Till 2016) via plagioclase-liquid geothermometry (Putirka 2008) and 876±29°C via QUILF two-pyroxene geothermometry.

Lava Creek Tuff and Huckleberry Ridge Tuff, Yellowstone

The Lava Creek Tuff is the product of the third, and most recent, caldera-forming eruption at Yellowstone that blanketed much of the continental United States in ash ca. 6.31 ka

(Matthews et al. 2015). The Lava Creek Tuff is dominantly composed of two members, LCT-A and LCT-B, which are indistinguishable in age and separated by a layer of fallout ash (Christiansen 2001). High-Fe, low-Al clinopyroxene (Table 4, Supplementary Table 3) were described in both members by Hildreth (1984). The new clinopyroxene-liquid geothermometer calculates temperatures for LCT-A and LCT-B of 805 and 776°C, respectively. These temperatures correspond within error with geothermometry of other LCT-B phases, sanidine: 814±23°C via the Putirka (2008) alkali feldspar-liquid geothermometer and quartz: 815±25°C via TitaniQ (Shamloo and Till 2017), as well as an LCT-B magma storage temperature of 800±50°C determined using the rhyolite-MELTS geothermometer (Gualda and Ghiorso 2015; Befus et al. 2018). Hildreth (1981) conducted Fe-Ti oxide geothermometry of both members, calculating ~800°C for LCT-A and ~950°C for LCT-B, implying a thermal gradient in the magma body similar to that proposed for the Bishop Tuff. However, the new clinopyroxene-liquid temperatures are just within uncertainty of each other, and do not support the interpretation of a thermal gradient. The Putirka (2008, Eq. 33) clinopyroxene-liquid geothermometer does not return temperatures for any of these natural samples, reinforcing the utility of the new geothermometer.

The Putirka (2008, Eq. 33) clinopyroxene-liquid geothermometer does return temperatures for clinopyroxene-liquid pairs from the Huckleberry Ridge Tuff, which was erupted during Yellowstone's first caldera-forming eruption ca. 2.1 Ma (Christiansen 2001), and contains compositionally similar clinopyroxene to that of the Lava Creek Tuff. The new clinopyroxene-liquid geothermometer returns a temperature for Huckleberry Ridge of 769°C, which is more than 30°C lower than the Putirka (2008, Eq. 33) geothermometer and below the rhyolite-MELTS-calculated liquidus for this system when modeled at 4.7 wt% H_2O (Gualda et al. 2012;

386 Myers et al. 2016). A clinopyroxene-liquid temperature of 769°C is also consistent with two-
387 feldspar geothermometry for the ignimbrite of 768–855°C (Elkins and Grove 1990; Swallow et
388 al. 2018). The new clinopyroxene-liquid temperatures for these large siliceous tuffs ≤ 800°C
389 implies that these minerals were last crystallizing at near-solidus conditions and at relatively high
390 crystal/liquid ratios.
391
392 **Implications**
393 In general, the new clinopyroxene-liquid geothermometer lowers calculated temperatures
394 for a given sample by an average of almost 90°C relative to prior clinopyroxene-liquid
395 geothermometers (Figure 4). In all cases where experiments are available, the temperature
396 returned by the new geothermometer is between the solidus and liquidus for the relevant bulk
397 composition—indicating that the new clinopyroxene-liquid geothermometer is a better
398 approximation of the relevant geologic conditions than the Putirka (2008, Eq. 33)
399 geothermometer, which consistently returns temperatures above the experimental liquidi or the
400 clinopyroxene-in phase boundaries of silicic magmas. Thus, the new geothermometer reconciles
401 many inconsistencies in previous thermometric results.
402 It is important to note that clinopyroxene chemistry and stability in high-silica systems is
403 not the same as in mafic systems. Dry experiments on mafic bulk compositions reveal that
404 clinopyroxene is stable from ~1470–1180°C at 1 atm to 25 kbar and is usually stable in these
405 experiments to at least 25° below its first appearance (e.g., Bartels et al. 1991; Elthon and Scarfe
406 1984; Feig et al. 2010, 2006; Grove et al. 1992; Grove and Juster 1989; Juster et al. 1989;
407 Kinzler and Grove 1992), whereas experiments on silicic bulk compositions that constrain
408 clinopyroxene stability are exclusively hydrous and restrict clinopyroxene stability to below

409 1000°C (e.g., Almeev et al. 2012; Bolte et al. 2015; Gardner et al. 2014; Iacovino et al. 2015). In
410 dry mafic systems above 11 kbar, clinopyroxene is rarely a liquidus phase and may become
411 unstable 25–40° after its first appearance (e.g., Bartels et al. 1991; Elthon and Scarfe 1984; Feig
412 et al. 2010, 2006; Grove et al. 1992; Grove and Juster 1989; Juster et al. 1989; Kinzler and Grove
413 1992). Conversely, in high-silica systems, experiments often place clinopyroxene on the liquidus
414 (Almeev et al. 2012; Gardner et al. 2014; Bolte et al. 2015; Iacovino et al. 2015). And although
415 clinopyroxene is a mafic phase, experiments and our temperature calculations demonstrate that
416 its stability is not restricted to near-liquidus temperatures; we have calculated clinopyroxene in
417 high-silica natural systems to below 775°C for the Late-erupted Bishop Tuff, Paektu comendite,
418 and Bandelier Tuff (Figure 4, Table 4), and experiments have shown the mineral to crystallize at,
419 or near, the solidus to temperatures as low as 675°C (e.g., Almeev et al. 2012; Befus and
420 Gardner 2016; Bolte et al. 2015; Gardner et al. 2014; Iacovino et al. 2015). If clinopyroxene
421 stability extends from the liquidus to the solidus in high-silica magma, the presence of
422 clinopyroxene does not necessitate the invocation of xenocrysts, mixing with a hotter magma
423 body, nor imply a low (or high) crystallinity. Instead, clinopyroxene, when present, appears to be
424 a persistent phase throughout the crystallization interval of high-silica systems.

425 Because of the lack of relevant experiments in its calibration dataset, thermodynamic
426 phase equilibria modeling of clinopyroxene-bearing systems using rhyolite-MELTS remains
427 problematic. Although Rhyolite-MELTS produces a realistic clinopyroxene crystallization
428 interval—that is, one consistent with the new geothermometer's temperature—for the Bishop
429 Tuff (Figure 5), it should be noted that Rhyolite-MELTS was calibrated for this particular
430 locality and the model does not perform as well for other high-silica systems. Rhyolite-MELTS
431 modeling often places clinopyroxene in the middle of, or late in, the high-silica system

This is a preprint, the final version is subject to change, of the American Mineralogist (MSA)
Cite as Authors (Year) Title. American Mineralogist, in press.
DOI: https://doi.org/10.2138/am-2019-6842

crystallization sequence, rather than on the liquidus as suggested by experiments (e.g., Almeev et al. 2012; Gardner et al. 2014; Iacovino et al. 2015). Rhyolite-MELTS failed to predict crystallization of clinopyroxene for 70% of the systems examined for this work, all of which contain clinopyroxene in the equilibrium mineral assemblage. For the trials in which clinopyroxene was predicted (not including the Bishop Tuff), on average rhyolite-MELTS predicted the clinopyroxene-in phase boundary over 120°C below the temperatures returned by the new clinopyroxene-liquid geothermometer and experimental phase equilibria, where available. We join other workers in urging caution when using rhyolite-MELTS to simulate systems in which clinopyroxene is present (e.g., Gardner et al. 2014), as its failure to accurately simulate the mineral's behavior may give the mistaken impression that clinopyroxene has a much narrower crystallization interval than in reality, as well as suggest an inaccurate degree of crystallinity.

Finding low-Al clinopyroxene in a lava may be evaluative in and of itself. In high-silica systems, clinopyroxene contains < 2 wt% Al_2O_3 (Figure 1), while it is possible for mafic clinopyroxene to contain > 10 wt% Al_2O_3, when compositions are queried from the GEOROC database. The low Al content in rhyolitic clinopyroxene is a result of a need for more Si in tetrahedral sites to compensate for the charge imbalance with O_3 oxygens produced by low Ca content in the crystal (CaO can be < 17 wt% in rhyolitic clinopyroxene and up to > 23 wt% in basaltic clinopyroxene; data from GEOROC) (Salviulo et al. 2000). Thus, the presence of low-Al clinopyroxene outside of a rhyolite may indicate that the mineral has been inherited from a higher-silica magma or country rock.

Low-Al, high-Fe clinopyroxene may also hint at the thermal history of the lava. Clinopyroxene high in Al have been linked to fast crystal growth and thus high undercooling;

455 during this process the crystal grows faster than the melt can deliver nutrients to the growth
456 surface, causing a depletion of compatible elements in the surrounding melt as well as an
457 enrichment in incompatible elements. As the crystal grows, it incorporates more incompatible
458 elements into its structure, causing an increase in these elements rim-ward (Lofgren et al. 2006;
459 Zhang 2008; Mollo and Hammer 2017). Conversely, crystal rims low in incompatible and high
460 in compatible elements as described herein counterindicate interface-controlled growth and
461 instead imply diffusion-controlled growth wherein the diffusive velocity of elements in the melt
462 is sufficient to deliver the ideal nutrients to the crystal. Additionally, experimental studies on
463 basaltic compositions have correlated low Al with slow cooling rates (e.g., Mollo et al. 2010).
464 The above suggests a slow growth rate for the low-Al, high-Fe clinopyroxene found in high-
465 silica magmatic systems, relative to high-Al clinopyroxene (Zhang 2008). This, combined with
466 our new geothermometer and clinopyroxene's broad stability in high-silica magmatic systems,
467 makes the mineral an attractive tool for investigating a range of processes in these hazardous
468 geological settings.
469

This is a preprint, the final version is subject to change, of the American Mineralogist (MSA)
Cite as Authors (Year) Title. American Mineralogist, in press.
DOI: https://doi.org/10.2138/am-2019-6842

Acknowledgements

Special thanks to Tim Grove for the use of the experimental petrology lab at MIT, and to Wes Hildreth for sharing his unpublished probe data. Additional thanks to Axel Wittmann, Kayla Iacovino, Jessica Noviello, Crystylynda Fudge, and the EPIC group at ASU. Great appreciation to Keith Putirka whose thoughtful questions and insights have helped guide this research. This work was supported by the National Park Services research permit YELL-2015-SCI-6078 and by the United States National Science Foundation under Graduate Research Fellowship #026257-001 to K.K.B. and CAREER EAR-1654584 to C.B.T. The EPMA facilities at ASU are in part supported by the National Nanotechnology Coordinated Infrastructure grant ECCS-1542160.

References Cited

Almeev, R.R., Bolte, T., Nash, B.P., Holtz, F., Erdmann, M., and Cathey, H.E. (2012) High-temperature, low-H2O Silicic Magmas of the Yellowstone Hotspot: an Experimental Study of Rhyolite from the Bruneau-Jarbidge Eruptive Center, Central Snake River Plain, USA. Journal of Petrology, 53, 1837–1866.

Anderson, A.T., Davis, A.M., and Lu, F. (2000) Evolution of Bishop Tuff Rhyolitic Magma Based on Melt and Magnetite Inclusions and Zoned Phenocrysts. Journal of Petrology, 41, 449–473.

Anderson, D.J., Lindsley, D.H., and Davidson, P.M. (1993) QUILF: A pascal program to assess equilibria among Fe, Mg, Mn, Ti oxides, pyroxenes, olivine, and quartz. Computers & Geosciences, 19, 1333–1350.

Bartels, K.S., Kinzler, R.J., and Grove, T.L. (1991) High pressure phase relations of primitive high-alumina basalts from Medicine Lake volcano, northern California. Contributions to Mineralogy and Petrology, 108, 253–270.

Befus, K.S., and Gardner, J.E. (2016) Magma storage and evolution of the most recent effusive and explosive eruptions from Yellowstone Caldera. Contributions to Mineralogy and Petrology, 171.

Befus, K.S., Bruyere, R.H., and Manga, M. (2018) Lava Creek Tuff Love. Presented at the Goldschmidt, Boston, MA, USA.

499 Bindeman, I.N., and Valley, J.W. (2002) Oxygen isotope study of the Long Valley magma
500 system, California: isotope thermometry and convection in large silicic magma bodies.
501 Contributions to Mineralogy and Petrology, 144, 185–205.

502 Bindeman, I.N., Fu, B., Kita, N.T., and Valley, J.W. (2008) Origin and Evolution of Silicic
503 Magmatism at Yellowstone Based on Ion Microprobe Analysis of Isotopically Zoned
504 Zircons. Journal of Petrology, 49, 163–193.

505 Bolte, T., Holtz, F., Almeev, R., and Nash, B. (2015) The Blacktail Creek Tuff: an analytical and
506 experimental study of rhyolites from the Heise volcanic field, Yellowstone hotspot
507 system. Contributions to Mineralogy and Petrology, 169.

508 Cashman, K.V., and Giordano, G. (2014) Calderas and magma reservoirs. Journal of
509 Volcanology and Geothermal Research, 288, 28–45.

510 Chamberlain, K.J., Morgan, D.J., and Wilson, C.J.N. (2014) Timescales of mixing and
511 mobilisation in the Bishop Tuff magma body: perspectives from diffusion chronometry.
512 Contributions to Mineralogy and Petrology, 168.

513 Christiansen, R.L. (2001) The Quaternary and Pliocene Yellowstone Plateau volcanic field of
514 Wyoming, Idaho, and Montana, 145 p. U.S. Geological Survey, Reston, Va.

515 Christiansen, R.L., Lowenstern, J.B., Smith, R.B., Heasler, H., Morgan, L.A., Nathenson, M.,
516 Mastin, L.G., Muffler, L.J.P., and Robinson, J.E. (2007) Preliminary Assessment of
517 Volcanic and Hydrothermal Hazards in Yellowstone National Park and Vicinity p. 94.
518 USGS.

519 Elkins, L.T., and Grove, T.L. (1990) Ternary feldspar experiments and thermodynamic models.
520 American Mineralogist, 75, 544–559.

521 Elthon, D., and Scarfe, C.M. (1984) High-pressure phase equilibria of a high-magnesian basalt
522 and the genesis of primary oceanic basalts. American Mineralogist, 69, 1–15.

523 Feig, S.T., Koepke, J., and Snow, J.E. (2006) Effect of water on tholeiitic basalt phase equilibria:
524 an experimental study under oxidizing conditions. Contributions to Mineralogy and
525 Petrology, 152, 611–638.

526 ——— (2010) Effect of oxygen fugacity and water on phase equilibria of a hydrous tholeiitic
527 basalt. Contributions to Mineralogy and Petrology, 160, 551–568.

528 Frost, B.R., and Lindsley, D.H. (1992) Equilibria among Fe-Ti oxides, pyroxenes, olivine, and
529 quartz: Part II. Application. American Mineralogist, 77, 1004–1020.

530 Gardner, J.E., Befus, K.S., Gualda, G.A.R., and Ghiorso, M.S. (2014) Experimental constraints
531 on rhyolite-MELTS and the Late Bishop Tuff magma body. Contributions to Mineralogy
532 and Petrology, 168.

533 Ghiorso, M.S., and Evans, B.W. (2008) Thermodynamics of Rhombohedral Oxide Solid
534 Solutions and a Revision of the FE-TI Two-Oxide Geothermometer and Oxygen-
535 Barometer. American Journal of Science, 308, 957–1039.

536 Ghiorso, M.S., and Gualda, G.A.R. (2013) A method for estimating the activity of titania in
537 magmatic liquids from the compositions of coexisting rhombohedral and cubic iron–
538 titanium oxides. Contributions to Mineralogy and Petrology, 165, 73–81.

539 Girard, G., and Stix, J. (2009) Magma Recharge and Crystal Mush Rejuvenation Associated with
540 Early Post-collapse Upper Basin Member Rhyolites, Yellowstone Caldera, Wyoming.
541 Journal of Petrology, 50, 2095–2125.

542 Girard, G., and Stix, J. (2010) Rapid extraction of discrete magma batches from a large
543 differentiating magma chamber: the Central Plateau Member rhyolites, Yellowstone
544 Caldera, Wyoming. Contributions to Mineralogy and Petrology, 160, 441–465.

545 Grove, T.L., and Juster, T.C. (1989) Experimental investigations of low-Ca pyroxene stability
546 and olivine-pyroxene-liquid equilibria at 1-atm in natural basaltic and andesitic liquids.
547 Contributions to Mineralogy and Petrology, 103, 287–305.

548 Grove, T.L., Kinzler, R.J., and Bryan, W.B. (1992) Fractionation of Mid-Ocean Ridge Basalt
549 (MORB). Geophysical Monograph, 71, 281–310.

550 Gualda, G.A.R., and Ghiorso, M.S. (2013) The Bishop Tuff giant magma body: an alternative to
551 the Standard Model. Contributions to Mineralogy and Petrology, 166, 755–775.

552 ——— (2015) MELTS_Excel: A Microsoft Excel-based MELTS interface for research and
553 teaching of magma properties and evolution. Geochemistry, Geophysics, Geosystems, 16,
554 315–324.

555 Gualda, G.A.R., and Sutton, S.R. (2016) The Year Leading to a Supereruption. (A.K. Schmitt,
556 Ed.)PLOS ONE, 11, e0159200.

Gualda, G.A.R., Ghiorso, M.S., Lemons, R.V., and Carley, T.L. (2012) Rhyolite-MELTS: a Modified Calibration of MELTS Optimized for Silica-rich, Fluid-bearing Magmatic Systems. Journal of Petrology, 53, 875–890.

Hervig, R.L., and Dunbar, N.W. (1992) Cause of chemical zoning in the Bishop (California) and Bandelier (New Mexico) magma chambers. Earth and Planetary Science Letters, 111, 97–108.

Hildreth, E.W. (1977) The magma chamber of the Bishop Tuff: Gradients in temperature, pressure, and composition. Ph.D. thesis, University of California, Berkeley.

Hildreth, W. (1981) Gradients in silicic magma chambers: Implications for lithospheric magmatism. Journal of Geophysical Research: Solid Earth, 86, 10153–10192.

Hildreth, W., and Wilson, C.J.N. (2007) Compositional Zoning of the Bishop Tuff. Journal of Petrology, 48, 951–999.

Hildreth, W., Christiansen, R.L., and O'Neil, J.R. (1984) Catastrophic isotopic modification of rhyolitic magma at times of caldera subsidence, Yellowstone Plateau Volcanic Field. Journal of Geophysical Research: Solid Earth, 89, 8339–8369.

Horn, S., and Schmincke, H.-U. (2000) Volatile emission during the eruption of Baitoushan Volcano (China/North Korea) ca. 969 AD. Bulletin of Volcanology, 61, 0537–0555.

Huang, R., and Audétat, A. (2012) The titanium-in-quartz (TitaniQ) thermobarometer: A critical examination and re-calibration. Geochimica et Cosmochimica Acta, 84, 75–89.

576 Huebner, J.S. (1980) Pyroxene phase equilibria at low pressure. In C.T. Preweitt, Ed., Pyroxenes
577 Vol. 7. Mineralogical Society of America.

578 Iacovino, K., Kim, J.S., Sisson, T.W., Lowenstern, J.B., Jang, J.N., Song, K.H., Ham, H.H., Ri,
579 K.H., Donovan, A.R., Oppenheimer, C., and others (2015) New Constraints on the
580 Geochemistry of the Millennium Eruption of Mount Paektu (Changbaishan), Democratic
581 People's Republic of Korea/China. In 2015 GSA Fall Meeting. San Francisco, CA, USA.

582 Iacovino, K., Kim, J.-S., Sisson, T., Lowenstern, J., Ri, K.-H., Jang, J.-N., Song, K.-H., Ham, S.-
583 H., Oppenheimer, C., Hammond, J.O.S., and others (2016) Quantifying gas emissions
584 from the "Millennium Eruption" of Paektu volcano, Democratic People's Republic of
585 Korea/China. Science Advances, 2, 1–11.

586 Juster, T.C., Grove, T.L., and Perfit, M.R. (1989) Experimental constraints on the generation of
587 FeTi basalts, andesites, and rhyodacites at the Galapagos Spreading Center, 85°W and
588 95°W. Journal of Geophysical Research, 94, 9251.

589 Kinzler, R.J., and Grove, T.L. (1992) Primary magmas of mid-ocean ridge basalts 1.
590 Experiments and methods. Journal of Geophysical Research, 97, 6885.

591 Liang, Y., Sun, C., and Yao, L. (2013) A REE-in-two-pyroxene thermometer for mafic and
592 ultramafic rocks. Geochimica et Cosmochimica Acta, 102, 246–260.

593 Lindsley, D.H. (1983) Pyroxene thermometry. American Mineralogist, 68, 477–493.

594 Lindsley, D.H., and Andersen, D.J. (1983) A two-pyroxene thermometer. Journal of Geophysical
595 Research, 88, A887.

596 Lofgren, G.E., Huss, G.R., and Wasserburg, G.J. (2006) An experimental study of trace-element
597 partitioning between Ti-Al-clinopyroxene and melt: Equilibrium and kinetic effects
598 including sector zoning. American Mineralogist, 91, 1596–1606.

599 Masotta, M., Mollo, S., Freda, C., Gaeta, M., and Moore, G. (2013) Clinopyroxene–liquid
600 thermometers and barometers specific to alkaline differentiated magmas. Contributions to
601 Mineralogy and Petrology, 166, 1545–1561.

602 Matthews, N.E., Vazquez, J.A., and Calvert, A.T. (2015) Age of the Lava Creek supereruption
603 and magma chamber assembly from combined ^{40}Ar/ ^{39}Ar and U-Pb dating of sanidine
604 and zircon crystals. Geochemistry, Geophysics, Geosystems, n/a-n/a.

605 Mollo, S., and Hammer, J.E. (2017) Dynamic crystallization in magmas. In W. Heinrich and R.
606 Abart, Eds., Mineral reaction kinetics: Microstructures, textures, chemical and isotopic
607 signatures Vol. 16, pp. 378–418. Mineralogical Society of Great Britain & Ireland.

608 Mollo, S., Del Gaudio, P., Ventura, G., Iezzi, G., and Scarlato, P. (2010) Dependence of
609 clinopyroxene composition on cooling rate in basaltic magmas: Implications for
610 thermobarometry. Lithos, 118, 302–312.

611 Myers, M.L., Wallace, P.J., Wilson, C.J.N., Morter, B.K., and Swallow, E.J. (2016) Prolonged
612 ascent and episodic venting of discrete magma batches at the onset of the Huckleberry
613 Ridge supereruption, Yellowstone. Earth and Planetary Science Letters, 451, 285–297.

614 Pamukcu, A.S., Gualda, G.A.R., and Anderson, A.T. (2012) Crystallization Stages of the Bishop
615 Tuff Magma Body Recorded in Crystal Textures in Pumice Clasts. Journal of Petrology,
616 53, 589–609.

617 Pamukcu, A.S., Ghiorso, M.S., and Gualda, G.A.R. (2016) High-Ti, bright-CL rims in volcanic
618 quartz: a result of very rapid growth. Contributions to Mineralogy and Petrology, 171.

619 Putirka, K.D. (2008) Thermometers and Barometers for Volcanic Systems. Reviews in
620 Mineralogy and Geochemistry, 69, 61–120.

621 Putirka, K.D., Mikaelian, H., Ryerson, F., and Shaw, H. (2003) New clinopyroxene-liquid
622 thermobarometers for mafic, evolved, and volatile-bearing lava compositions, with
623 applications to lavas from Tibet and the Snake River Plain, Idaho. American
624 Mineralogist, 88, 1542–1554.

625 Reid, M.R., Vazquez, J.A., and Schmitt, A.K. (2011) Zircon-scale insights into the history of a
626 Supervolcano, Bishop Tuff, Long Valley, California, with implications for the Ti-in-
627 zircon geothermometer. Contributions to Mineralogy and Petrology, 161, 293–311.

628 Sack, R.O., and Ghiorso, M.S. (1994) Thermodynamics of multicomponent pyroxenes: II. Phase
629 relations in the quadrilateral. Contributions to Mineralogy and Petrology, 116, 287–300.

630 Salviulo, G., Secco, L., Marzoli, A., Piccirillo, E.M., and Nyobe, J.B. (2000) Ca-rich pyroxene
631 from basic and silicic volcanic rocks from the Cameroon Volcanic Line (West-Africa):
632 crystal chemistry and petrological relationships. Mineralogy and Petrology, 70, 73–88.

633 Shaffer, J.S., and Till, C.B. (2016) New Temperature and H2O Estimates for Post Caldera
634 Yellowstone Rhyolite Lavas using Feldspar Geothermometry and Rhyolite-MELTS. In
635 2016 AGU Fall Meeting. San Francisco, CA, USA.

636 Shamloo, H.I., and Till, C.B. (2017) Petrologic Insights into the Timing and Triggering
637 Mechanism of the Lava Creek Tuff Supereruption, Yellowstone Caldera, WY, USA. In
638 2017 IAVCEI Scientific Assembly p. 995. Presented at the IAVCEI, Portland, OR.

639 Sisson, T.W. (1991) Pyroxene-high silica rhyolite trace element partition coefficients measured
640 by ion microprobe. Geochimica et Cosmochimica Acta, 55, 1575–1585.

641 Swallow, E.J., Wilson, C.J.N., Myers, M.L., Wallace, P.J., Collins, K.S., and Smith, E.G.C.
642 (2018) Evacuation of multiple magma bodies and the onset of caldera collapse in a
643 supereruption, captured in glass and mineral compositions. Contributions to Mineralogy
644 and Petrology, 173.

645 Till, C.B., Vazquez, J.A., and Boyce, J.W. (2015) Months between rejuvenation and volcanic
646 eruption at Yellowstone caldera, Wyoming. Geology, 43, 695–698.

647 Vazquez, J.A., Kyriazis, S.F., Reid, M.R., Sehler, R.C., and Ramos, F.C. (2009)
648 Thermochemical evolution of young rhyolites at Yellowstone: Evidence for a cooling but
649 periodically replenished postcaldera magma reservoir. Journal of Volcanology and
650 Geothermal Research, 188, 186–196.

651 Wark, D.A., and Watson, E.B. (2006) TitaniQ: a titanium-in-quartz geothermometer.
652 Contributions to Mineralogy and Petrology, 152, 743–754.

653 Wark, D.A., Hildreth, W., Watson, E.B., and Cherniak, D.J. (2004) Origin of Thermal and
654 Compositional Zoning in the Bishop Magma Reservoir: Insights from Zoned Quartz
655 Phenocrysts p. 3. Presented at the 2004 AGU Fall Meeting, San Francisco, CA, USA.

Wark, D.A., Hildreth, W., Spear, F.S., Cherniak, D.J., and Watson, E.B. (2007) Pre-eruption recharge of the Bishop magma system. Geology, 35, 235.

Warshaw, C.M., and Smith, R.L. (1988) Pyroxenes and fayalites in the Bandelier Tuff, New Mexico: temperatures and comparison with other rhyolites. American Mineralogist, 73, 1025–1037.

Wilcock, J., Goff, F., Minarik, W.G., and Stix, J. (2013) Magmatic Recharge during the Formation and Resurgence of the Valles Caldera, New Mexico, USA: Evidence from Quartz Compositional Zoning and Geothermometry. Journal of Petrology, 54, 635–664.

Wilson, C.J.N., and Hildreth, W. (1997) The Bishop Tuff: New Insights From Eruptive Stratigraphy. The Journal of Geology, 105, 407–440.

Zhang, Y. (2008) Geochemical Kinetics, 631 p. Princeton University Press, Princeton, New Jersey.

669 ## Figure Captions

670

671 **Figure 1.** Clinopyroxene compositions from experiments and silicic igneous systems. Gray
672 symbols: clinopyroxene used to calibrate existing geothermometers (Sack and Ghiorso 1994,
673 Putirka personal communication). Black solid and matching black outlined symbols:
674 clinopyroxene used to calibrate and test the new clinopyroxene-liquid geothermometer (Almeev
675 et al. 2012; Gardner et al. 2014; Bolte et al. 2015; Iacovino et al. 2015). Colored symbols:
676 compositions of clinopyroxene from natural high-silica magmatic systems (Hildreth 1977;
677 Warshaw and Smith 1988; Sisson 1991; Girard and Stix 2009; Gardner et al. 2014; Iacovino et
678 al. 2016). Inset: Pyroxene quadrilateral of the same clinopyroxene as the main figure.

679

680 **Figure 2.** Clinopyroxene crystallized during CSPV experiment SCL01-3 (775°C 1 kbar 572 hrs).
681 Crystals used for calibration indicated with white arrows. Gray background is glass.

682

683 **Figure 3.** Calculated vs. experimental temperature. Temperatures are calculated using both the
684 Putirka (2008, Eq. 33) clinopyroxene-liquid geothermometer (open symbols) and the new
685 geothermometer (solid green symbols), and are plotted against the experimental conditions.
686 Symbols are the same for both panels. The solid line represents unity between the calculated and
687 experimental temperatures. Dashed lines show the best fit through each dataset to better illustrate
688 the new geothermometer's efficacy. (**a**) Calibration data. Arrow emphasizes that in the
689 temperature range of most interest for high-silica magmatic systems, temperatures calculated
690 with the new geothermometer are consistently closer to unity. (**b**) Test data.

691

692 **Figure 4.** Natural clinopyroxene temperatures calculated with clinopyroxene-liquid
693 geothermometers. Average ΔT is 84°C. Compositional data from [a] Hildreth (1977) and Gardner
694 et al. (2014), [b] Warshaw and Smith (1988) and Wilcock et al. (2013), [c] Iacovino et al. (2016), [d]
695 Sisson (1991), [e] Girard and Stix (2010), and [f] Befus and Gardner (2016) and Girard and Stix
696 (2010) available in Supplementary Table 3.
697
698 **Figure 5.** Comparison of temperatures and clinopyroxene stability for the Late-erupted Bishop
699 Tuff (Ig2). Clinopyroxene-liquid (Putirka 2008, Eq. 33), two-pyroxene (Frost and Lindsley
700 1992), two-feldspar (Chamberlain et al. 2014), and quartz-magnetite oxygen isotope (Bindeman
701 and Valley 2002) temperatures all are higher than the experimental liquidus/clinopyroxene-in of
702 Gardner et al. (2014). Fe-Ti oxide (Frost and Lindsley 1992) and TitaniQ (Wark et al. 2004,
703 2007) temperature ranges straddle this liquidus (white square = average TitaniQ temperature).
704 The clinopyroxene-liquid temperature of this work is below the experimental liquidus, consistent
705 with the rhyolite-MELTS clinopyroxene-in, and is more consistent with the Gardner et al. (2014)
706 Bishop Tuff pre-eruptive storage temperature and Ti in zircon temperature (Gualda and Ghiorso
707 2013) than the Putirka (2008, Eq. 33) clinopyroxene-liquid temperature.
708

Tables

Table 1 Experiment starting glass

Oxide	wt%	st.dev.
SiO_2	74.59	2.73
TiO_2	0.23	0.15
Al_2O_3	13.75	1.96
Cr_2O_3	0.01	0.01
FeO^{tot}	1.75	0.71
MnO	0.04	0.03
MgO	0.19	0.09
CaO	1.03	0.34
Na_2O	2.55	0.37
K_2O	5.15	0.19

EPMA data; n = 14.

Table 2 CSPV experimental conditions

Experiment	T (°C)	P (kbar)	t (hrs)
SCL01-4	750	1.0	573
SCL01-3	775	1.0	572
SCL01-5	800	1.0	385
SCL01-1	825	1.0	410

Table 3 Calibration dataset experimental conditions

Locality	n	T (°C)	P (kbar)
Scaup Lake rhyolite	4	750–825	1.0
Cougar Point and Indian Batt rhyolites[a]	36	875–1025	2.0–5.0
Blacktail Creek rhyolite tuff[b]	4	790–850	2.0
Late-erupted Bishop Tuff pumice[c]	10	700–800	1.0–2.0
Paektu Millennium comendite pumice[d]	10	675–750	0.5–1.5

Composition data from [a] Almeev et al. (2012), [b] Bolte et al. (2015), [c] Gardner et al. (2014), and [d] Iacovino et al. (2015) are available in Supplementary Table 2.

Table 4 Average natural clinopyroxene compositions and clinopyroxene-liquid temperatures. Standard deviation in italics for this work.

Locality	SiO_2	TiO_2	Al_2O_3	Cr_2O_3	FeO^{tot}	MnO	MgO	CaO	Na_2O	K_2O	T (°C)
Scaup Lake	51.56	0.17	0.64	0.01	15.42	0.75	11.13	19.97	0.32	0.03	800
	0.26	*0.02*	*0.04*	*0.01*	*0.51*	*0.05*	*0.23*	*0.24*	*0.02*	*0.01*	
South Biscuit Basin[a]	51.81	0.19	0.68	0.00	16.54	0.84	10.76	18.87	0.29	0.02	793
Solfatara Plateau[b]	49.34	0.22	0.48	0.00	26.37	0.87	4.12	18.29	0.30	0.01	771
Bishop Tuff[c]	51.98	0.15	0.74	0.00	12.82	0.57	12.69	20.65	0.38	0.00	759
Paektu Millennium[d]	48.94	0.22	0.20	0.00	28.75	0.88	0.86	18.46	1.70	0.00	755
Lava Creek Tuff A[e]	48.95	0.20	0.64	0.00	25.11	0.71	5.59	18.48	0.32	0.00	805
Lava Creek Tuff B[e]	48.57	0.23	0.62	0.00	26.68	0.73	4.48	18.38	0.31	0.00	776
Huckleberry Ridge Tuff[f]	48.49	0.20	0.60	0.00	27.40	0.86	3.28	18.89	0.30	0.00	769
Bandelier Tuff[g]	52.08	0.14	0.51	0.00	22.19	1.97	7.10	15.46	0.56	0.00	780

Oxides given in wt% and normalized. SEE for temperature calculations is ±20°C. Complete data from [a] Girard and Stix (2010), [b] Girard and Stix (2010) and Befus and Gardner (2016), [c] Hildreth (1977) and Gardner et al. (2014), [d] Iacovino et al. (2016), [e] Hildreth, personal communication, [f] Sisson (1991), and [g] Warshaw and Smith (1988) are available in Supplementary Table 3.

Figure 2

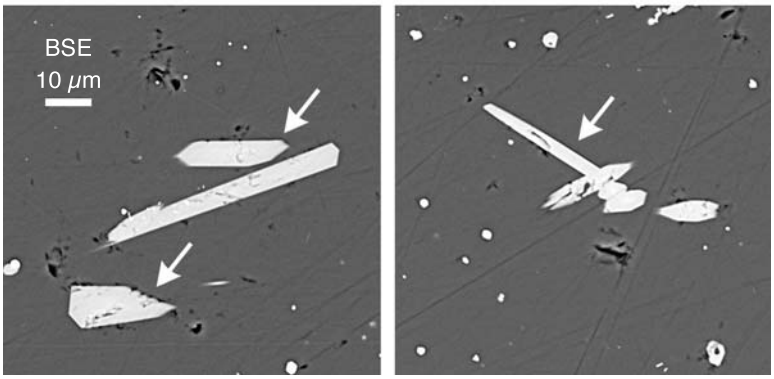

Figure 5

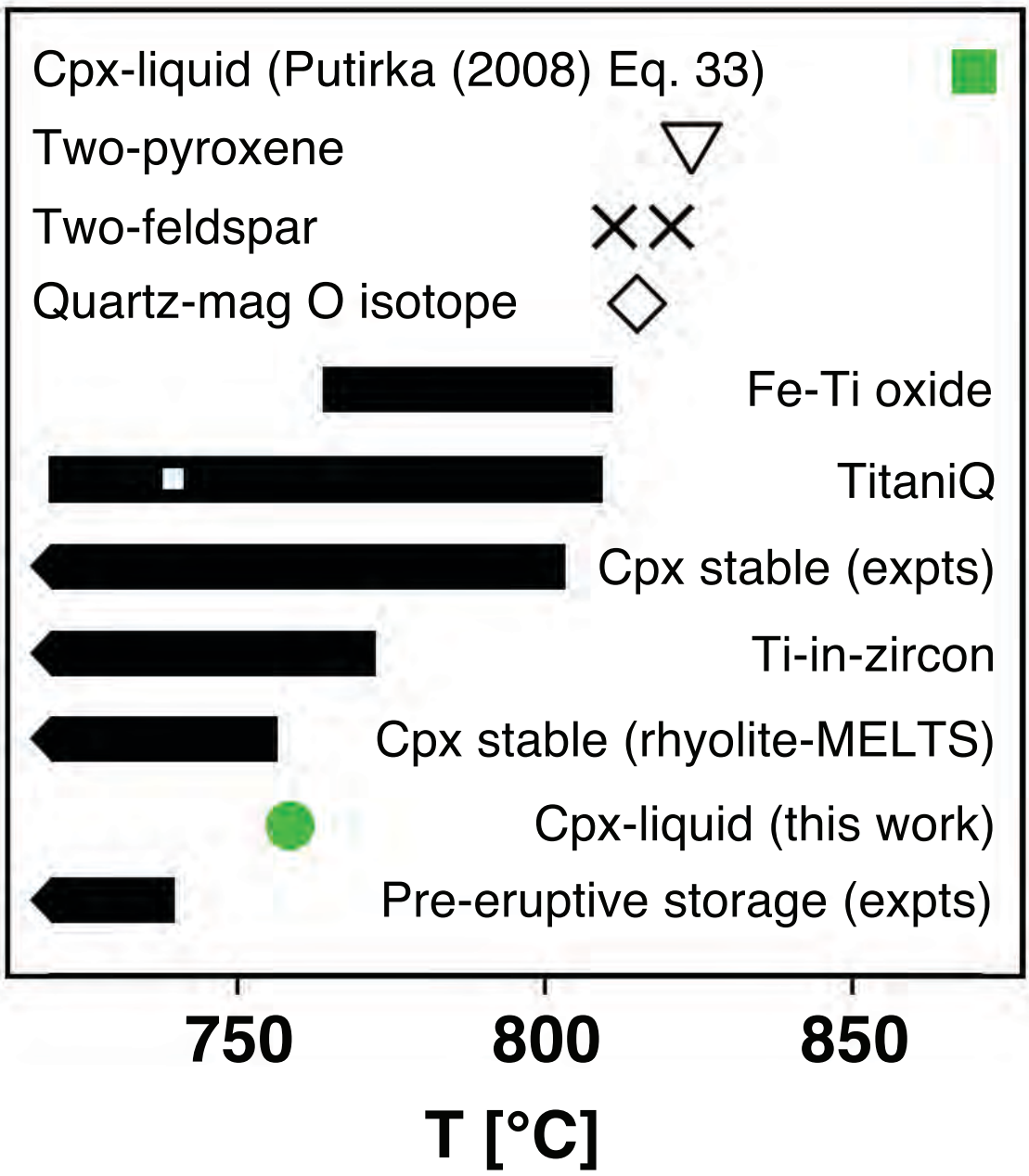
Cpx-liquid (Putirka (2008) Eq. 33)
Two-pyroxene
Two-feldspar
Quartz-mag O isotope
Fe-Ti oxide
TitaniQ
Cpx stable (expts)
Ti-in-zircon
Cpx stable (rhyolite-MELTS)
Cpx-liquid (this work)
Pre-eruptive storage (expts)
750
800
850
T [°C]

Figure 1

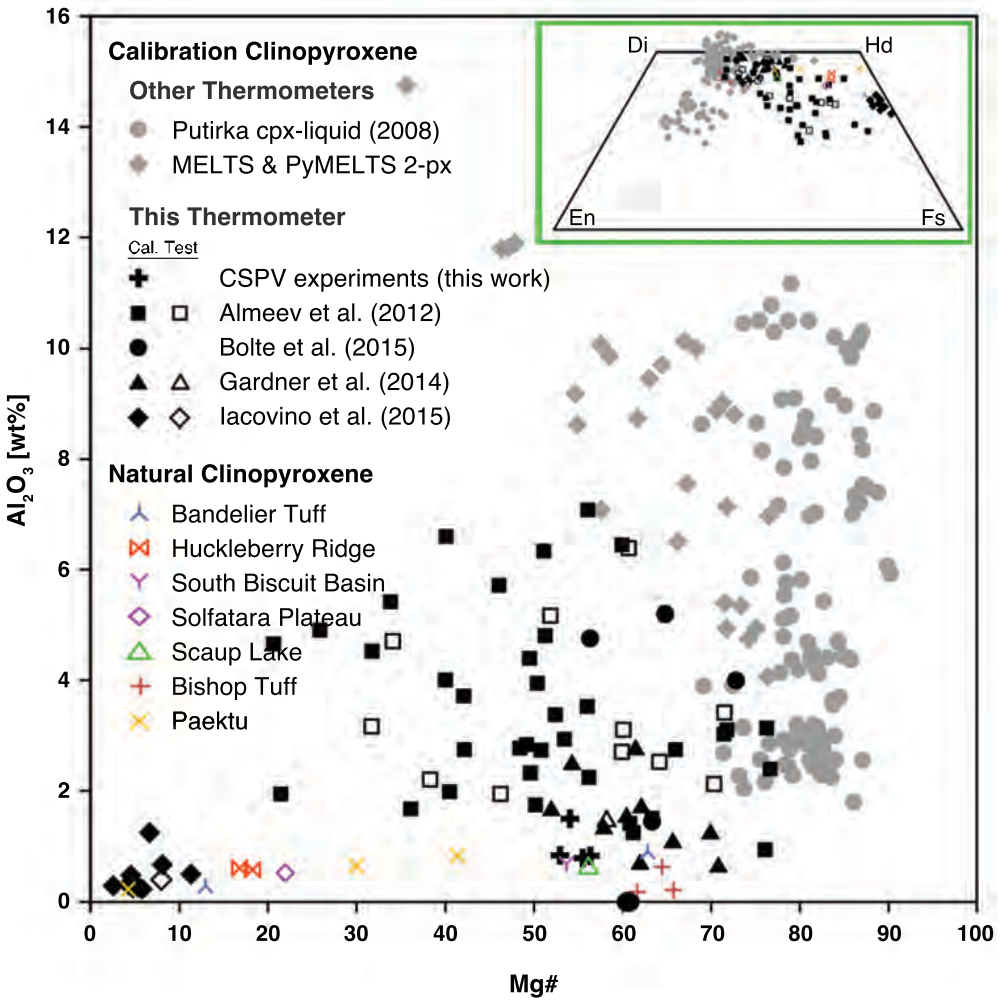
Calibration Clinopyroxene
Other Thermometers
Putirka cpx-liquid (2008)
MELTS & PyMELTS 2-px
This Thermometer
Cal. Test
CSPV experiments (this work)
Almeev et al. (2012)
Bolte et al. (2015)
Gardner et al. (2014)
Iacovino et al. (2015)
Natural Clinopyroxene
Bandelier Tuff
Huckleberry Ridge
South Biscuit Basin
Solfatara Plateau
Scaup Lake
Bishop Tuff
Paektu
Di
Hd
En
Fs
Al2O3 [wt%]
Mg#
0
2
4
6
8
10
12
14
16
0
10
20
30
40
50
60
70
80
90
100

Figure 3

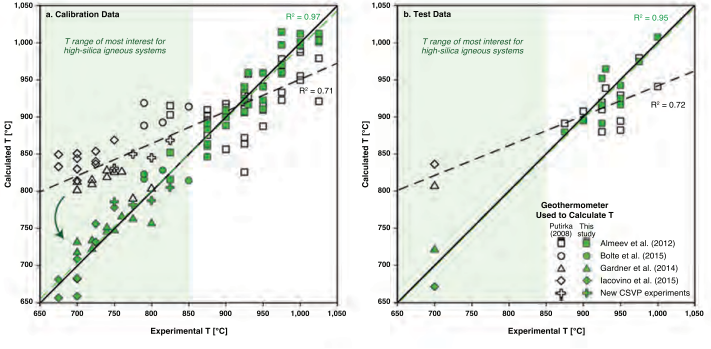
a. Calibration Data
R² = 0.97
T range of most interest for high-silica igneous systems
R² = 0.71
Calculated T [°C]
Experimental T [°C]
b. Test Data
R² = 0.95
T range of most interest for high-silica igneous systems
R² = 0.72
Geothermometer Used to Calculate T
Putirka (2008)
This study
Almeev et al. (2012)
Bolte et al. (2015)
Gardner et al. (2014)
Iacovino et al. (2015)
New CSVP experiments
650
700
750
800
850
900
950
1,000
1,050

Figure 4

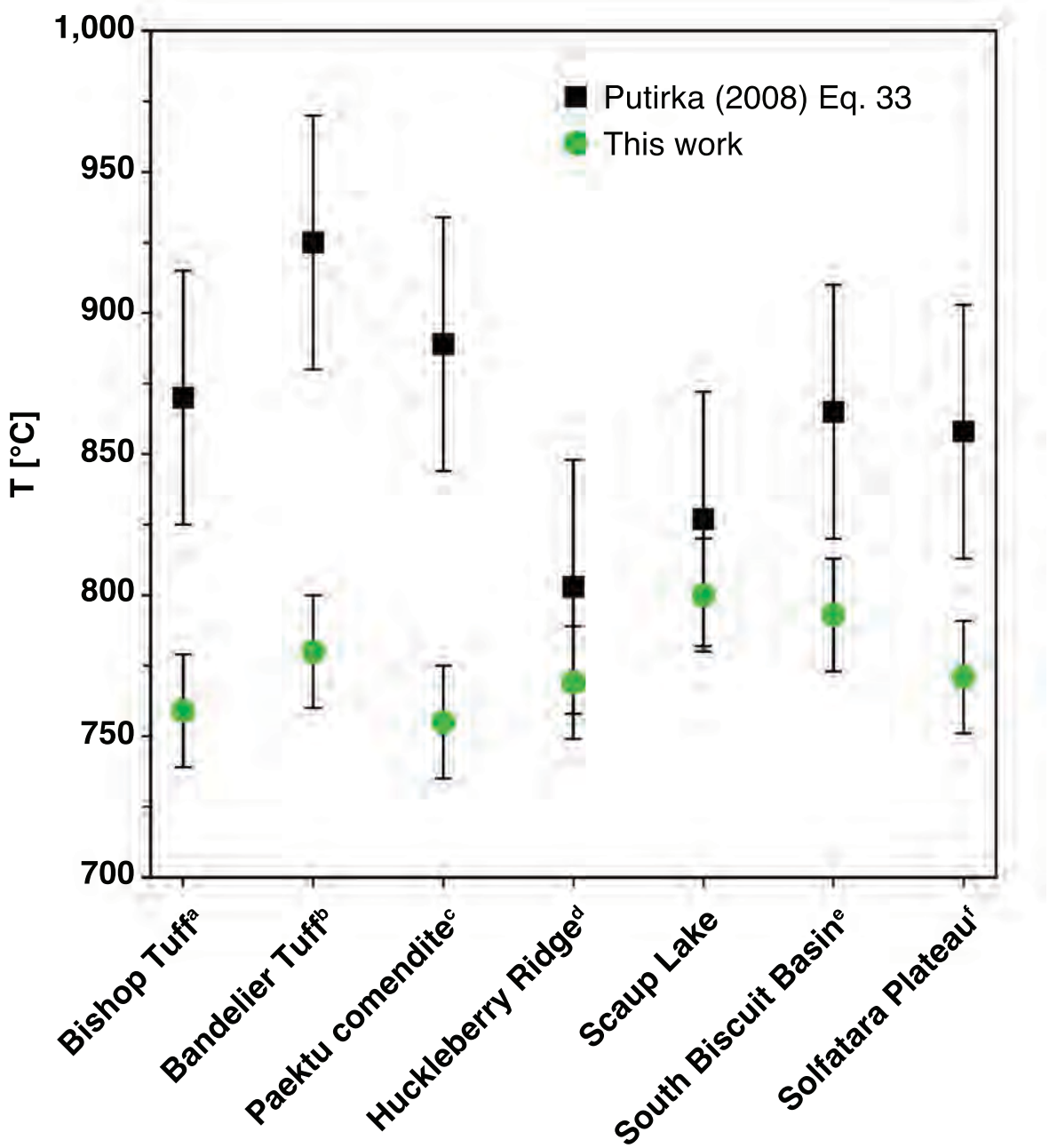
1,000
950
900
850
800
750
700
T [°C]
Putirka (2008) Eq. 33
This work
Bishop Tuff[a]
Bandelier Tuff[b]
Paektu comendite[c]
Huckleberry Ridge[d]
Scaup Lake
South Biscuit Basin[e]
Solfatara Plateau[f]